Paulina Trybek*, Michał Nowakowski and Lukasz Machura

Evaluation of the training objectives with surface electromyography

DOI 10.1515/bams-2015-0035
Received September 25, 2015; accepted January 11, 2016; previously published online February 19, 2016

Abstract: In this work, the multifractal analysis of the kinesiological surface electromyographic signal is proposed. The goal was to investigate the level of neuromuscular activation during complex movements on the laparoscopic trainer. The basic issue of this work concerns the changes observed in the signal obtained from the complete beginner in the field of using laparoscopic tools and the same person subjected to the series of training. To quantify the complexity of the kinesiological surface electromyography, the nonlinear analysis technique, namely, the multifractal detrended fluctuation analysis, was adopted. The analysis was based on the parameters describing the multifractal spectrum – the Hurst exponent – and the spectrum width. The statistically significant differences for a selected group of muscles at the different states (before and after training) are presented. In addition, as the base case, the relaxation state was considered and compared with the working states.

Keywords: electromyography; hurst exponent; multifractal analysis.

Introduction

The improper patterns of muscle recruitment are often the cause for the decrease of the efficiency of the movements in many aspects of life. This automatically entails reduction of the precision and is also the reason for an increasing fatigue [1, 2]. This work concerns the issue of the ergonomic handling of the laparoscopic instruments. At the moment, most of the assessments are performed subjectively by a trainer either locally or, in some rare cases, remotely using video assessment tools. These methods lack both repeatability and specificity. The effectiveness of the surface electromyography (sEMG) in the assessment of the level of involvement of the muscular system has some strong evidence [3–5]. However, some relevant and unsolved issues need to be addressed. To compare the signal of a muscle activation at the different levels of involvement for the selected individual muscle groups located in the human arms, a simple experiment was invented. As its details will be presented in the next section, here we will only mention that we have recorded the sEMG signals from the untrained and trained volunteers. The detected differences in the signals received from the volunteers performing complex movements on laparoscopic trainer can open new opportunities of using sEMG as a helpful tool in the process of the individual training in rather difficult motor tasks. Several works documenting the physiological phenomena and focusing on the nonlinear dynamics, including chaos theory and fractal behavior, have been reported in the last few years [6–11]. Physiological signals are highly complex and, therefore, require an appropriate analysis, which will be able to bring us closer to the understanding of the true nature of the process (or processes) behind the signal. Traditional analysis, mainly based on the conventional statistical tests of mean, median, etc., may not be sufficient (see, for instance, the series of articles of analysis of the cardiac rhythm [12, 13]), as the important information embedded in the signal could be easily lost. In addition, for the description of the neuromuscular activation during functional movements, the influence of the neighboring muscles due to the location of the electrodes over the group of muscles and the modification of the source position in relation to each electrodes are the main difficulties with the data interpretation [14]. In the discussed case, the multifractal detrended fluctuation analysis (MFDFA) was applied. The proposed method is based on the scaling properties of fluctuations in the time series. MFDFA developed by Kantelhardt et al. [15, 16] became a popular method for the wide range of application for the study of the nonlinear phenomena [7]. This includes aspects of the biomedical signal analysis [17, 18], which is the case presented here. The paper is organized as follows: Section 2 describes the experimental method. In Section 3, the MFDFA method for data analysis is introduced. The results are presented

***Corresponding author: Paulina Trybek,** Institute of Physics, University of Silesia, Katowice, Poland, E-mail: p.trybek@us.edu.pl
Michał Nowakowski: Department of Medical Education, Faculty of Medicine, Jagiellonian University Medical College, Kraków, Poland
Lukasz Machura: Institute of Physics, University of Silesia, Katowice, Poland; and Silesian Center for Education and Interdisciplinary Research, University of Silesia, Chorzów, Poland

in Section 4. The last section summarizes the results and draws conclusions.

Subjects and methods

Subjects and task

Six volunteers (equal gender distribution, three males and three females), 24–27 years of age, with similar physical conditions were recruited for the experiment. The experiment was conducted on a laparoscopic trainer (see Figure 1). All participants were right-handed. Novice users had to tie surgical knots using an intracorporeal double-handed technique. The knots were tied on the metal half rings using a 15-cm-long surgical thread. The task was to tie the largest possible numbers of knots in the allotted time. There were two measurement points: (1) at the beginning of the experiment and (2) after a series of training events. The average time required to learn the proper technique took around 3 h (three series of training, 60 min each).

Experimental data

To quantify the results of the experiment, the sEMG method was chosen. Muscular activity was recorded from the four groups of muscles on each arm. The selected groups potentially exhibit the largest level of an excessive tension and constitute the main muscle sets engaged in the performed task. The electrodes were located around separated groups of muscles, namely, trapezius ridge, deltoids, forearm – long palmar muscle and ulnar wrist flexor, thenar eminence – abductor muscle of thumb, and flexor brevis. We used bipolar concentric surface AgCl electrodes, 15×15 mm in size, with a concentrating connector. The interelectrode distance was set to 1 cm. Concentric electrodes were used to compensate the difficulties with the proper placement of electrodes in relation to the direction of muscular fibers and also to compensate the changes related to the morphology of the shape of the action potential during the movement. We took an extra effort to precisely localize the electrodes over the belly of the muscle to avoid the influence from the adjacent muscles and to reduce the cross talk. The measurements were conducted using the eight-channel sEMG recorder (OT Bioelettrinica, Torino, IT). The system automatically records the mean value of the electromyogram signal over a time interval of 125 ms. The average rectified value measured in microvolts was collected in the maximum voluntary contraction mode. The measurement was performed for the complete relaxed state and during the movements before and after the training series. For all these states, usual recording time took around 45 min.

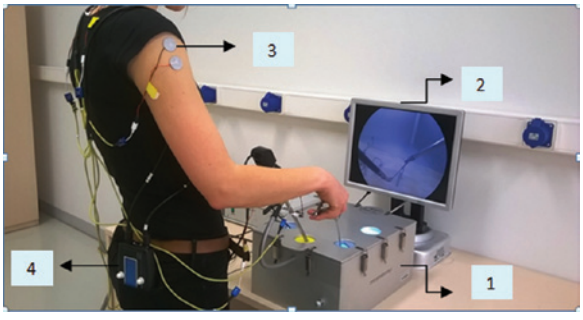

Figure 1: A volunteer working on a laparoscopic trainer; 1 – laparoscopic box, 2 – preview of the performed task, 3 – pair of electrodes, and 4 – measuring device.

Data analysis

The recorded difference of the electric potential present on the skin, which in turn is related to the action potentials propagating along the muscle fibers, will be a main source of the analyzed data. As usual, the idea was to find quantifiers that will allow to justify the actual state of the group of muscles. We are mainly concerned with the possibility of comparison of the two states: untrained and trained volunteers. The central result of multifractal analysis is a multifractal spectrum (MF spectrum). The complete procedure and the detailed step-by-step numerical scheme can be found in the studies of Kantelhardt et al. [15, 16] and Ihlen [19]. Here we will only present the general idea of the MFDFA method and describe the parameters of interest.

Multifractal spectrum

The essential aspect of the fractal (and multifractal) analysis lies in self-similarity. The time series $x(t)$ observed at a time scale t is said to be statistically self-similar with the time series $x(kt)$ observed at k times longer time scale kt when the following relation is fulfilled:

$$x(kt) \equiv k^H x(t). \tag{1}$$

The exponent H characterizes the type of self-similarity. Equation 1 describes the system for which the magnification of a small part is not statistically different from the whole.

The self-similar (self-affine) time series is often expressed as a fractal, but in less rigorous terminology (for details, see [16, 20, 21]). The development of methods for estimating self-similarity exponents has enabled a possibility for the precise description of the complex multiscale organization of the signal, even if the signal itself cannot be regarded as a fractal in a strict sense [21]. MFDFA is one of the several methods widely used to calculate a set of similarity exponents. This method is based on the analysis of the scaling properties of the signal's fluctuations. It offers a scheme to obtain the MF spectrum, which indicates the frequency of the occurrence of the singularities.

In the following paragraphs, we will introduce the typical MFDFA, as presented by Kantelhardt et al. [15] and Ihlen [19]. In short, the analysis requires the following stages: Suppose that we have time series with N data points $\{x_i\}_1^N$, then we perform four consecutive steps:

(i) Calculate the profile y_i as the cumulative sum from the data with the subtracted mean

$$y_i=\sum_{k=1}^{i}[x_i-\langle x\rangle]. \tag{2}$$

(ii) The cumulative signal is split into N_s equal nonoverlapping segments of size s. Here, for the length of the segments, we use the power of two, $s=2^r$. Typically, the exponent r would range from 4 to $\lfloor \log_2(N/10)\rfloor$. However, the minimum sample size must be larger than the polynomial order to prevent the overfitting of the polynomial trend. The use of $N/10$ for the upper limit means that at least 10 segments will be used in the calculations. Larger segment sizes will result in rather weak statistics. Usually, the length of the data will not be accordant with the power of two, and some data parts would have to be dropped from the analysis. Therefore, the same procedure should be performed starting from the last index, and in turn the $2N_s$ segments will be taken into account.

(iii) Calculate the local trend $y_{v,i}^m$ for the vth segment by means of the least-square fit of order m. Then determine the variance,

$$F^2(s,v)\equiv\frac{1}{s}\sum_{i=1}^{s}(y_{v,i}^m-y_{v,i})^2, \tag{3}$$

for each segment $v=1,\ldots,N_s$. The same procedure has to be repeated in the reversed order (starting from the last index). Next, determine the fluctuation function being the qth statistical moment of the calculated variance:

$$F_q(s)=\left(\frac{1}{2N_s}\sum_{v=1}^{2N_s}[F^2(s,v)]^{\frac{q}{2}}\right)^{\frac{1}{q}},\quad q\neq 0, \tag{4}$$

$$F_0(s)=\exp\left\{\frac{1}{4N_s}\sum_{v=1}^{2N_s}\ln[F^2(s,v)]\right\},\quad q=0. \tag{5}$$

The previously mentioned function needs to be calculated for all segment size s. We have exploited several different orders of the fitted polynomials and end up with no statistical difference between the results. Here we will present the analysis with the quadratic fit.

(iv) In the last step, the determination of the scaling law of the fluctuation function (Equation 4) is performed by means of the log-log plots of $F_q(s)$ versus segment size s for all values of q. The function $F_q(s)\sim s^{h(q)}$ is naturally smaller for the smaller fluctuations, which results in the increasing function with the increasing segment size. From the $h(q)$ called the generalized Hurst exponent, we are able to determine several quantifies. First, we work out the mass exponent using the formula

$$\tau(q)=qh(q)-1. \tag{6}$$

The mass exponent $\tau(q)$ is used to calculate a q-order singularity exponent $\alpha=\tau'(q)$. This quantity is also known as a Hölder exponent. From the previous equation, the q-order singularity dimension,

$$D(q)=q\alpha-\tau(q)=q[\alpha-h(q)]+1, \tag{7}$$

can be constructed. The singularity dimension $D(q)$ is related to the mass exponent $\tau(q)$ by the Legendre transform.

The MF spectrum shown schematically in Figure 2 identifies the deviation of the fractal structure within the periods for large and small fluctuation [19]. The rare events are defined as the smallest values of the generalized Hurst exponent $h(q)$ located at the left end of the spectrum. In the quantitative description of the spectrum, we would like to concentrate on the spectrum

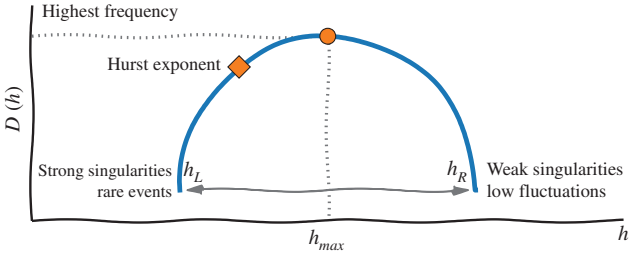

Figure 2: Schematic picture of the MF spectrum with the characteristic parameters: spectrum width, Hurst exponent, and h_{max} (the most probable singularity).

width $\Delta=h_R-h_L$ and the global Hurst exponent H (or self-similarity exponent).

These values describe crucial properties for the recorded signals. The spectrum width determines the diversity of periods with the different scales (for high and low fluctuations). The values of the Hurst exponent describe the nature of noise found in the time series. The range of the Hurst exponent values can be interpreted [6, 15, 19] as follows: $h\in(0, 0.5)$ indicates the antipersistency of the signals, $h=0.5$ represents an uncorrelated noise, and $h\in(0.5, 1)$ indicates the persistency of the series. This interpretation of the entire signal is valid only if the data exhibit the monofractal character. For the multifractal systems, the set of the exponents is needed, which is caused by the local characteristic of the fluctuations. The shape of the MF spectrum itself has a wide and meaningful interpretation [13, 19].

Results

Despite many advantages offered by the MFDFA method in the application to the complex biomedical data, some particular steps require users to have individual decisions that can have significant effect on the final results. The main issue concerns the choice of the scaling range s for the proper estimation of the fluctuation function $F_q(s)$ (Equation 4). In the literature, one can find some useful advices for the appropriate selection the range of the scales [6, 19].

The length of the analyzed time series N consists of around 21,000 data points. For the calculations presented in this work, the scales (segments length) $s\in(64,512)$ and typical $q\in(-5, 5)$ were chosen. The examples of the double logarithmic dependence $F_q(s)$ versus s together with the corresponding MF spectra are presented in the Figure 3. Within the selected range of scales, the linear dependence of the fluctuation function $F_q(s)$ on the segment length s can be observed. Also, it can be noticed that for the presented working states (before and after the training), the spectrum is relatively wide, and there is no significant difference between the values of the MF spectrum width before and after training.

Spectrum width

The mean values of the spectral width are presented in Table 1. Channels are assigned to each group of muscles. C_1–C_4 represent the left arm, and C_5–C_8 indicate muscles from the right arm. C_1 and C_5 form a pair of the respective trapezius ridge group of muscles located on the left and right arms. Similarly, channels C_2 and C_6 record signals from the deltoids, C_3 and C_7 from the forearm muscle group (long palmar muscle and ulnar wrist flexor), and finally C_4 and C_8 from the group of thenar muscles.

The smallest value of the spectrum width for each channel occurs at the relaxation state. The Wilcoxon test at the significance level of $\alpha=0.05$ was used to compare the relaxation state with the work states before and after the

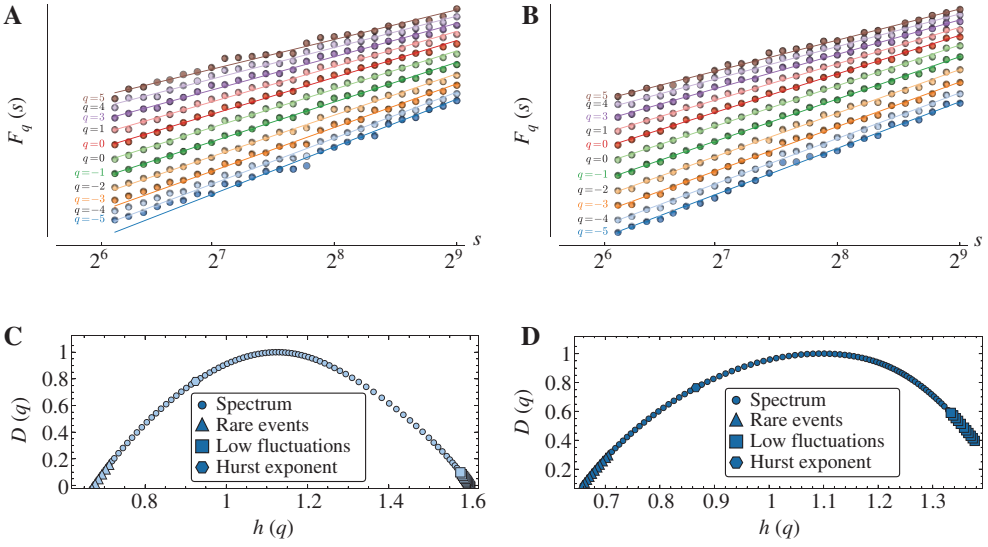

Figure 3: The example of double logarithmic dependence $F_q(s)$ versus s together with the corresponding MF spectra presented for the forearm muscle group from the right hand (C_6).
(A) [$F_q(s)$ before training], (B) [$F_q(s)$ after training], (C) [MF spectrum before training], (D) [MF spectrum after training].

Table 1: Mean values of the spectrum width for all channels and at each state.

	Average spectrum width ⟨Δ⟩							
Channel number	C_1	C_2	C_3	C_4	C_5	C_6	C_7	C_8
Relaxation	0.3±0.074	0.564±0.058	0.35±0.13	0.743±0.054	0.233±0.068	0.441±0.147	0.39±0.11	0.794±0.108
Before training	0.58±0.14	0.577±0.103	1.204±0.235	1.865±0.33	0.465±0.078	0.778±0.114	1.095±0.164	1.063±0.2
After training	0.761±0.216	0.987±0.14	1.126±0.1	1.488±0.22	0.574±0.15	0.504±0.14	1.187±0.155	1.147±0.174

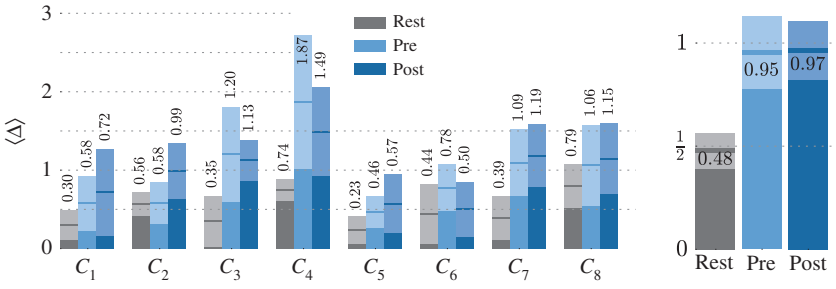

Figure 4: Mean values of the spectral width Δ.
Left panel: comparison of mean values for the individual groups of muscles (see text for details). Right panel: comparison of the mean values for three different states – at rest, before the training, and after the training. Numbers refer to the actual values of means. The confidence interval is depicted with the slightly lightened colors for each bar separately.

training. With the exception of C_5 and C_8, all other channels indicate a statistical significance at the selected level ($p<0.05$). This effect is clearly apparent in the right panel of Figure 4, where the mean values of the MF spectrum ⟨Δ⟩ calculated from all the channels in the three states (rest, pretraining, and posttraining) are presented. The left diagram in Figure 4 suggests the similar characteristic of the spectrum width for the corresponding muscles in the right and left arms. For the series obtained before and after the training, the highest value of the MF spectrum width occurs for the groups of the forearm (C_3 and C_7) and thenar (C_4 and C_8) muscles (see Table 1 for details). The spectrum width can serve as an effective predictor for the identification of the relaxation state of the muscle activity. By contrast, the width Δ alone cannot distinguish between the working states before and after the training.

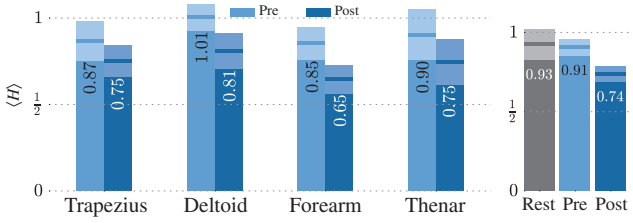

Figure 5: Mean values of the Hurst exponent.
Left panel: comparison of mean values for the individual groups of muscles (see text for details). Right panel: comparison of the mean values for three different states – at rest, before the training, and after the training. Bars indicate standard deviations. Numbers refer to the actual values of means. The confidence interval is depicted with the slightly lightened colors for each bar separately.

Hurst exponent

The most important aspect of this work was the identification of the statistically different parameters, which could be applied to distinguish between the signals obtained from the skilful and inexperienced student. This quantifiers could then be used for the automatic evaluation of one's ability of handling laparoscopic tools. First, we would like to focus on these two working states (pretraining and posttraining) by means of the Hurst exponent H. In contrast to the just analyzed width ⟨Δ⟩, the mean Hurst exponent ⟨H⟩ indicates the statistical difference between the data recorded before and after the training (cf. Figure 5). We grouped together the values for the corresponding clusters of muscles from the left and right arm for all six volunteers and calculated the arithmetic mean values of the Hurst exponent ⟨H⟩ for the corresponding channels separately. These values are summarized in Table 2 and presented in the left panel of Figure 5. For all the muscle groups, the values of the Hurst exponent of the series after the training (post state) are significantly lower (see Figure 5). The statistical significance occurs for

Table 2: Average values of the Hurst exponent $\langle H \rangle$ for the corresponding groups of muscles for the left (C_1–C_4) and right (C_5–C_8) hand at each of the three recorded states.

			Average Hurst exponent $\langle H \rangle$	
Muscles group	**Trapezius ridge (C_1+C_5)**	**Deltoid (C_2+C_6)**	**Forearm (C_3+C_7)**	**Thenar (C_4+C_8)**
Relaxation/rest	0.791±0.071	0.894±0.097	0.715±0.055	1.304±0.057
Before training	0.868±0.053	1.006±0.035	0.853±0.043	0.904±0.067
After training	0.752±0.042	0.811±0.047	0.646±0.0376	0.749±0.06

deltoids (C_2 and C_6, with p=0.0096) and forearm (C_3 and C_7, with p=0.0077). The visual representation on this dependence is presented as the box plot in Figure 6.

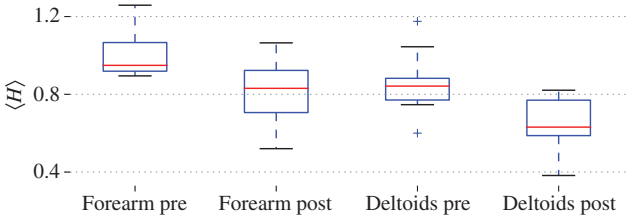

Figure 6: The box-and-whisker diagram of the average Hurst exponent $\langle H \rangle$ for two different groups of muscles at two different working states.
The average Hurst exponents were calculated for both arms together. The plot for the forearm muscle group (long palmar muscle and ulnar wrist flexor) is shown on two diagrams on the left hand side. The two diagrams on the r.h.s correspond to the deltoids. Pretraining and posttraining reflects the abilities of using the laparoscopic tools before and after the training, respectively. Boxes correspond to the estimated quartiles, and whiskers indicate a variability outside the upper and lower quartiles, i.e. the minimum and maximum values.

Thenar group of muscles

Upon the comparison of the signals acquired at rest and before the training sessions with those after the training, the significant difference of the calculated averages of the Hurst exponents can be seen. This result is demonstrated in the right panel of the Figure 5, where the mean values of Hurst exponent taken from the all the muscles together are presented for each of the states rest (gray), pretraining (light blue), and posttraining (blue). The dominant effect of this dissimilarity lies in the mean value of the Hurst exponent of the thenar muscles, which show a statistically significant (p=0.0037) increase in the exponent for the relaxation state separately. These findings were quite unexpected as they indicate the different characters of irregular component for the rest state of the discussed group of muscles alone. At the rest state, the value is relatively high $\langle H \rangle^{\text{rest}}_{C_4,C_5}$ =1.3037 and is typically assigned to the integrated noise (random walk) [19]. For all the other muscle groups, the relaxation states show the persistence characteristic [19], which is characteristic to the noisy nature of the time series (cf. Table 2).

The discussed cases are depicted in the Figure 7, which compares the individual raw signals that indicate the biggest difference of the Hurst exponent at the relaxation state. Figure 8 presents raw time series acquired from

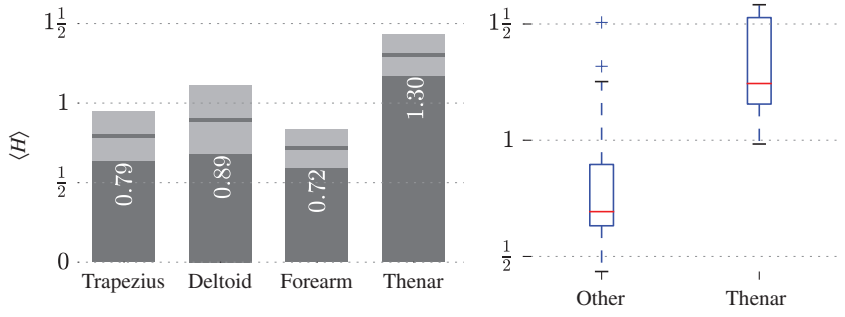

Figure 7: Average Hurst exponent presented for all groups of muscles calculated for both arms together.
The left panel shows bar chart for all of the groups separately. Please note that the thenar group of muscles possesses the highest Brownian motion-like value of $\langle H \rangle$. All other groups can be interpreted as noisy signals. The confidence interval is depicted with light gray for each bar separately. On the right hand side, the box-and-whisker diagram of the average Hurst exponent is compared for joined groups of the trapezius, deltoid, and forearm muscles versus the thenar group. Boxes correspond to the estimated quartiles, and whiskers indicate a variability outside the upper and lower quartiles, i.e. the minimum and maximum values.

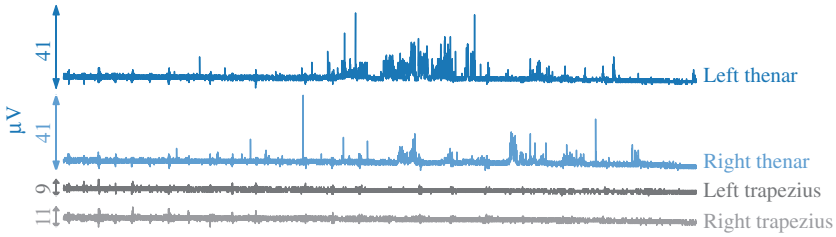

Figure 8: Exemplary raw sEMG signals acquired from one of the volunteers before the analysis.
The arrows present the ranges of the recorded values of the signal in microvolts. Groups of muscles from top to bottom: left thenar, right thenar, left trapezius, and right trapezius. The strong difference in the characteristic of the signals can be notice just by the naked eye.

one of the volunteers from four groups of muscles: left thenar, right thenar, left trapezius, and right trapezius (top to bottom). The differences in the muscle activity – significantly lower amplitudes for the trapezius ridge and much larger fluctuations for the thenar group – are clearly visible.

In addition, one can notice that for the thenar group, the average spectral width Δ also takes the highest values out of all muscle groups (see Table 1 for details).

This very muscle group exhibits several difficulties at the measurement. For instance, the tools constantly touch the skin and can also touch the electrodes from time to time. This might cause an excessive sweating, which in turn will influence the signal. The last issue is the area of the electrodes in relation to the area of the muscles. All of the previously mentioned conditions matter mainly at the work states, i.e. when the volunteer performs the actual task with the laparoscopic tools and are rather irrelevant for the rest state.

Conclusions

The signal from the sEMG recorded during the complex movements on the laparoscopic trainer was analyzed. The main goal was to find a statistical difference between the signals acquired before and after the training. In addition, the relaxation (rest) state was considered. To quantify the complexity of the series, the selected parameters that characterize an MF spectrum was used. The study of the spectral width does not allow to determine the differences in the pretraining and posttraining states but is sufficient to distinguish between rest and work states. Because of the small sample and also the necessity of using the nonparametric test, the statistical power of the test was lower. However, the investigation of the values of the Hurst exponent indicate that this parameter seems to be a better classifier between the analyzed states (before and after the training) than the MF spectrum width. For all of the examined muscle groups for both arms, the values of the Hurst exponent appear to be lower after the series of training; however, this difference is statistically significant only for the deltoid and forearm muscle groups. The rather unexpected finding is the characteristic of the thenar muscles. Both the value of the MF spectrum width and the global Hurst exponent are distant from all other groups at the rest state. In summary, it can be concluded that sEMG indicates a potential method for the evaluation of the complex dynamics of the action potential of the muscles. Research on the dynamical properties of sEMG signals is still at an early stage, where many aspects are waiting to be discovered.

Research funding: This work was partially supported by the JUMC research grant: K/ZDS/003962.
Author contributions: All the authors have accepted responsibility for the entire content of this submitted manuscript and approved submission.
Employment or leadership: None declared.
Honorarium: None declared.
Competing interests: The funding organization(s) played no role in the study design; in the collection, analysis, and interpretation of data; in the writing of the report; or in the decision to submit the report for publication.

References

1. Aggarwal R, Moorthy K, Darzi A. Laparoscopic skills training and assessment. Br J Surg 2004;91:1549–58.
2. Forsman M, Birch L, Zhang Q, Kadefors R. Motor unit recruitment in the trapezius muscle with special reference to coarse arm movements. J Electromyogr Kinesiol 2001;11:207–16.
3. Hug F. Can muscle coordination be precisely studied by surface electromyography? J Electromyogr Kinesiol 2011;21:1–12.
4. Merletti R, Parker PA. Electromyography: physiology, engineering, and noninvasive applications, volume 11. Hoboken, New Jersey: John Wiley & Sons, 2004.

5. Barbero M, Merletti R, Rainoldi A. Atlas of muscle innervation zones: understanding surface electromyography and its applications. Springer Science & Business Media, 2012.
6. Gierałtowski J, Żebrowski JJ, Baranowski R. Multiscale multifractal analysis of heart rate variability recordings with a large number of occurrences of arrhythmia. Phys Rev E Stat Nonlin Soft Matter Phys 2012;85:021915.
7. Goldberger AL. Non-linear dynamics for clinicians: chaos theory, fractals, and complexity at the bedside. Lancet 1996;347: 1312–4.
8. Hampson KM, Mallen EA. Multifractal nature of ocular aberration dynamics of the human eye. Biomed Opt Express 2011;2: 464–70.
9. Bryce RM, Sprague KB. Revisiting detrended fluctuation analysis. Sci Rep 2012;2:315.
10. Chowdhury RH, Reaz MB, Ali MA, Bakar AA, Chellappan K, Chang TG. Surface electromyography signal processing and classification techniques. Sensors 2013;13:12431–66.
11. Hakonen M, Piitulainen H, Visala A. Current state of digital signal processing in myoelectric interfaces and related applications. Biomed Signal Process Control 2015;18: 334–59.
12. Goldberger AL, Rigney DR, West BJ. Chaos and fractals in human physiology. Sci Am 1990;262:42–9.
13. Makowiec D, Gałąska R, Dudkowska A, Rynkiewicz A, Zwierz M. Long-range dependencies in heart rate signal – revisited. Physica A 2006;369:632–44.
14. Peter K. The ABC of EMG – a practical introduction to kinesiological electromyography. USA: Noraxon Inc, 2005.
15. Kantelhardt JW, Zschiegner SA, Koscielny-Bunde E, Havlin S, Bunde A, Stanley HE. Multifractal detrended fluctuation analysis of nonstationary time series. Physica A 2002;316:87–114.
16. Kantelhardt JW. Fractal and multifractal time series. In: Encyclopedia of complexity and systems science. New York: Springer-Verlag, 2009:3754–79.
17. Gupta V, Suryanarayanan S, Reddy NP. Fractal analysis of surface EMG signals from the biceps. Int J Med Inform 1997;45:185–92.
18. Ivanov PC, Amaral LA, Goldberger AL, Havlin S, Rosenblum MG, Struzik ZR, et al. Multifractality in human heartbeat dynamics. Nature 1999;399:461–5.
19. Ihlen EA. Introduction to multifractal detrended fluctuation analysis in Matlab. Front Physiol 2012;3:141.
20. Lakhtakia A, Messier R, Varadan VV, Varadan VK. Self-similarity versus self-affinity: the Sierpinski gasket revisited. J Phys A Math Gen 1986;19:L985.
21. Abry P, Gonçalves P, Lévy Véhel J. Scaling, fractals and wavelets. Digital signal and image processing series. London, UK: ISTE–John Wiley & Sons, Inc., 2009.